Acta Chemica Scandinavica, 1993: 47: 1162–1172
Printed in Belgium – all rights reserved

ACTA
CHEMICA SCANDINAVICA
ISSN 0904-213X

Simulating Impedance Spectra from a Mechanistic Point of View: Diffusion Effects in Metal Dissolution Reactions

Elisabet Ahlberg* and Helge Anderson

Department of Inorganic Chemistry, Chalmers University of Technology and University of Göteborg, S-412 96 Göteborg, Sweden

Ahlberg, E. and Anderson, H., 1993. Simulating Impedance Spectra from a Mechanistic Point of View: Diffusion Effects in Metal Dissolution Reactions. – Acta Chem. Scand. 47: 1162–1172. © Acta Chemica Scandinavica 1993.

The influence of diffusion on the impedance characteristics of metal dissolution reactions has been investigated. Simulated data are compared to experimental data on the dissolution of zinc in slightly acidic sulfate solutions. The simulations show that in the presence of adsorbed intermediates a specific coupling between the adsorption and diffusion processes occurs. This coupling remains even at anodic potentials and is rather insensitive to the hydrodynamic conditions. Thus, the absence of a rotation speed dependence on the impedance characteristics is not a sufficient criterion for assuming kinetic control. It is also shown that the experimental results can be interpreted as being a result of the coupling between the adsorption and diffusion processes.

Dissolution and deposition reactions of metals have been studied in great detail with impedance spectroscopy (IS).[1–5] The impedance spectra of these reactions usually show one or several relaxations (capacitive or inductive), which have been assigned to adsorbed intermediates participating in the reactions. Mass transport effects have been suppressed by the use of the rotating disc electrode (RDE). Methods for calculating the a.c. response in the absence[6,7] and in the presence[6] of diffusion have been developed. In the latter case it was shown that there exists a coupling between the adsorption and diffusion processes, which affects the impedance spectra. For reactions where the rate is controlled by semi-infinite diffusion of soluble species the impedance is characterised by the well known Warburg impedance with a unit slope in the complex impedance plane. In the presence of adsorbed intermediates the Warburg tail becomes distorted in its high-frequency part, owing to the coupling between adsorption and diffusion. With the use of a rotating disc electrode the Warburg impedance is usually assumed to be negligible. However, at frequencies where the coupling is important the impedance is relatively insensitive to changes in the mass transport conditions.

The purpose of the present study is to show the effects on the impedance when both adsorption of intermediates and diffusion of soluble species are taken into account.

Three dissolution/deposition mechanisms of metals have been simulated. The discussion of the results is focused on the coupling between the adsorption and the diffusion processes. The simulations show that the presence of adsorbed intermediates under certain conditions may reduce the possibility to eliminate the coupling effects between adsorption and diffusion in the impedance spectra by the use of a RDE at ordinary rotation speeds where ω_{RDE} is less than 100 revolutions per second (rps). Hence, the diffusion-adsorption impedance observed in the mid- or low-frequency part of the spectra becomes almost independent of the rotation speed if $\omega_{RDE} > 30$ rps. It is also shown that these coupling effects may occur at relatively large anodic potentials even if diffusion of ions towards the electrode is the only diffusion process considered (the dissolution reaction is not supposed to be diffusion limited). Together these effects may lead to misinterpretations of the impedance spectra, since kinetic control may be erroneously assumed.

The theoretical results are compared to an experimental impedance study of the zinc dissolution reaction in slightly acidic sulfate solutions. The zinc dissolution reaction has been studied with IS by several authors.[4,5,8,9] In these studies pure kinetic control was assumed and the observed relaxations in the low-frequency region of the spectra was thus assigned to adsorbed intermediates.

In the present study, the experimental results at anodic potentials show that the impedance spectra of the zinc reaction consist of one inductive and one capacitive loop besides the charge transfer loop. The spectra are, within experimental uncertainty, independent of ω_{RDE} when $\omega_{RDE} > 30$ rps. Thus, a plausible interpretation would be a charge-transfer process with at least two adsorbed inter-

* To whom correspondence should be addressed.

mediates participating in the reaction sequence. However, for experiments obtained at a stationary electrode, diffusion is clearly visible.

By considering the diffusion of Zn^{2+} and H^+ in the simulations, the capacitive loop in the experimental spectra could be interpreted as arising from diffusion, also under hydrodynamic conditions. Thus, in order to explain the experimental data, only one adsorbed intermediate of zinc is necessary in the reaction path.

Derivation of the impedance

Since the coupling between the adsorption of intermediates and the diffusion of soluble species is seldom considered in the impedance of metal dissolution reactions, the derivation of the impedance function is carried out in the present study. The resulting impedance function is general with respect to the number of adsorbed species and diffusing soluble species.

Consider an electrochemical interface where heterogeneous reactions can take place. The Faradaic current density, I_f, that flows through the interface is determined by the charge- and mass-balance equations (1) and (2), where z_n is the number of electrons transferred in the nth step. K_n and K_{-n} are the normalised forward and

$$I_f = F\sum_n z_n(K_n - K_{-n}) \tag{1}$$

$$\beta_i \frac{d\theta_i}{dt} = \sum_n (\nu_{i,n} - \nu_{i,-n}) \tag{2}$$

backward rate constants (in mol $cm^{-2}\,s^{-1}$), defined as the product of the rate constant, k_n or k_{-n}, and the concentration of reacting species. β_i is the maximum concentration of adsorbed species (in mol cm^{-2}) with the coverage θ_i, and $\nu_{i,n}$ is the rate of formation and disappearance of the adsorbed intermediate caused by the nth and $-n$th reaction steps. The rate constants k_n and k_{-n} are assumed to vary exponentially with the potential [eqns. (3) and (4)], where k_n^* and k_{-n}^* are the forward

$$k_n = k_n^* \exp\left(\frac{(1-\alpha)\,z_n F}{RT}(E - E_{ref})\right) \tag{3}$$

$$k_{-n} = k_{-n}^* \exp\left(\frac{-\alpha z_n F}{RT}(E - E_{ref})\right) \tag{4}$$

and backward rate constants at a reference potential E_{ref} common for all reaction steps. From this it follows that E° for different reaction steps may differ and that $E^\circ = E_{ref}$ only when $k_n^* = k_{-n}^*$. The rest of the symbols have their usual meaning. If the electrode, at steady state, is perturbed by a small sinusoidal potential signal $\Delta E = |\Delta E| \exp(j\omega t)$, where $j = \sqrt{-1}$, the potential dependent variables will respond in the same way, i.e. $\Delta\theta = |\Delta\theta| \exp(j\omega t)$ and $\Delta c = |\Delta c| \exp(j\omega t)$. The faradaic current, I_f, is obtained by a first-order Taylor expansion of the potential dependent variables, eqn. (5), where m is

$$\Delta I_f = \frac{\partial I}{\partial E}\Delta E + \sum_{i=1}^{m}\frac{\partial I}{\partial \theta_i}\Delta\theta_i + \sum_{k=m+1}^{n}\frac{\partial I}{\partial c_k}\Delta c_k \tag{5}$$

the number of adsorbed species and n the sum of adsorbed and soluble species. Division of eqn. (5) by ΔE yields the faradaic admittance, Y_f, the inverse of the impedance. The partial derivatives in eqn. (5) are easily obtained from the charge balance equation, eqn. (1). The variation of the coverage, $\Delta\theta_i$, with the potential perturbation can be obtained by noting that the total differential of the time-dependent variation of the coverage, eqn. (2), is equal to $j\omega\beta_i\Delta\theta_i$. Division by ΔE and β_i gives the linear equation (6) [or in matrix form eqn. (7)], which can be solved for $\Delta\theta_i/\Delta E$.

$$j\omega\frac{\Delta\theta_i}{\Delta E} = a_i + \sum_{j=1}^{m} J_{i,j}\frac{\Delta\theta_i}{\Delta E} + \sum_{k=m+1}^{n} R_{i,k}\frac{\Delta c_k}{\Delta E} \tag{6}$$

$$\begin{bmatrix} J_{1,1}-j\omega & J_{1,2} & \cdots\cdots & J_{1,m} \\ J_{2,1} & J_{2,2}-j\omega & \cdots\cdots & J_{2,m} \\ \cdots\cdots & \cdots\cdots & \cdots\cdots & \cdots\cdots \\ J_{m,1} & J_{m,2} & \cdots\cdots & J_{m,m}-j\omega \end{bmatrix} \begin{bmatrix} \frac{\Delta\theta_1}{\Delta E} \\ \frac{\Delta\theta_2}{\Delta E} \\ \cdots \\ \frac{\Delta\theta_m}{\Delta E} \end{bmatrix} = \begin{bmatrix} -a_1 - \sum_{k=m+1}^{n} R_{1,k}\frac{\Delta c_k}{\Delta E} \\ -a_2 - \sum_{k=m+1}^{n} R_{2,k}\frac{\Delta c_k}{\Delta E} \\ \cdots\cdots\cdots \\ -a_m - \sum_{k=m+1}^{n} R_{m,k}\frac{\Delta c_k}{\Delta E} \end{bmatrix} \tag{7}$$

where

$$a_i = \frac{\partial\left(\frac{d\theta_i}{dt}\right)}{\partial E};\quad J_{i,j} = \frac{\partial\left(\frac{d\theta_i}{dt}\right)}{\partial\theta_i};\quad R_{i,k} = \frac{\partial\left(\frac{d\theta_i}{dt}\right)}{\partial c_k}$$

Analytical solutions for kinetically controlled reactions with a maximum of three adsorbed intermediates have been presented earlier.[10] In that case the $\Delta c_k/\Delta E$ terms on the right-hand side of eqn. (7) are zero. The corresponding solutions when diffusion is taken into account can be expressed as eqn. (8) where $|J(\omega)|$ is the determinant of

$$\frac{\Delta\theta_i}{\Delta E} = \frac{\sum_{j=1}^{m}\left[(-1)^{(i+j)}\,|J(\omega)|_{j,i}\left(-a_j - \sum_{k=m+1}^{n} R_{j,k}\frac{\Delta c_k}{\Delta E}\right)\right]}{|J(\omega)|} \tag{8}$$

the J-matrix and $|J(\omega)|_{j,i}$ is the sub-determinant of the J-matrix when the jth row and ith column are excluded.

In the case of one adsorbed intermediate, $J(\omega) = J_{1,1} - j\omega$ and $|J(\omega)|_{1,1} = 1$. Δc_k is obtained from the time-dependent variation of the concentration at the electrode surface, which is determined by Fick's second law of diffusion. For a sine wave perturbation of a planar electrode it can be written as eqn. (9), where Δc_k is the concentration change

$$j\omega\Delta c_k(x) = D_k \frac{\partial^2 \Delta c_k(x)}{\partial x^2} \tag{9}$$

caused by the perturbation and D_k the diffusion coefficient of the species denoted k. The solution of eqn. (9) has been given for stationary conditions (semi-infinite diffusion) and for the rotating disc electrode (finite thickness of the diffusion layer) by eqn. (10), where N_k depends on

$$\Delta c_k(x=0) = \pm \frac{\Delta I_f}{F} N_k(\omega) \tag{10}$$

the thickness of the diffusion layer, and is given by eqn. (11) for an infinite diffusion layer and eqn. (12) for a

$$N_k(\omega) = 1/(j\omega D_k)^{1/2} \tag{11}$$

$$N_k(\omega) = \frac{\tanh[\delta_k(j\omega/D_k)^{1/2}]}{(j\omega D_k)^{1/2}} \tag{12}$$

finite diffusion layer. A positive sign in eqn. (10) applies to species diffusing towards the surface and a negative sign to species diffusing away from the surface (anodic current is defined as positive). The use of a rotating disc electrode allows calculation of the diffusion layer thickness, $\delta_k = 1.61 D_k^{1/3} \omega_{RDE}^{-1/2} \nu^{1/6}$.

If Δc_k is substituted into eqn. (5) and eqn. (8), the faradaic admittance can be obtained [eqn. (13), where Y_{ads}, C_1 and C_2 are given by eqns. (14)–(16), respectively]. Eqn. (13) is general with respect to the number of

$$Y_f = \frac{\Delta I_f}{\Delta E} = \frac{\dfrac{1}{R_{ct}} + Y_{ads}}{1 - C_1 - C_2} \tag{13}$$

$$Y_{ads} = \sum_{i=1}^{m} \frac{\partial I_f}{\partial \theta_i} \frac{\sum_{j=1}^{m} ((-1)^{(i+j-1)} |J(\omega)|_{j,i} a_j)}{|J(\omega)|} \tag{14}$$

$$C_1 = \frac{1}{F} \frac{\sum_{i=1}^{m} \left[\frac{\partial I_f}{\partial \theta_i} \sum_{j=1}^{m} \left((-1)^{(i+j-1)} |J(\omega)|_{j,i} \sum_{k=m+1}^{n} [R_{j,k} N_k(\omega)] \right) \right]}{|J(\omega)|} \tag{15}$$

$$C_2 = \frac{1}{F} \sum_{k=m+1}^{n} \left(\frac{\partial I_f}{\partial c_k} N_k(\omega) \right) \tag{16}$$

adsorbed intermediates and diffusing species. If all $N_k(\omega)$ are zero, eqn. (13) reduces to the numerator, which represents the impedance of pure kinetically controlled reactions. If no adsorbed intermediates are present the second term in both the numerator and the denominator disappears and the equation represents a charge-transfer resistance in series with a Warburg impedance. The coupling effect between the adsorption and diffusion processes, frequently mentioned later in the text, can be addressed to a large contribution of the C_1-term, eqn. (13), to the faradaic impedance. The total impedance, Z_t, is obtained by adding the double layer capacitance, C_{dl}, in parallel to the faradaic impedance [eqn. (17)].

$$Y_t = Y_f + j\omega C_{dl} \text{ or } Z_t = \frac{Z_f}{1 + j\omega Z_f C_{dl}} \tag{17}$$

Since the frequency dependence of the impedance may be rather complex, especially when several adsorbed intermediates are present, it is desirable to express the impedance with frequency-independent parameters which can be calculated outside the repetitive frequency loop in the computer algorithm. In the appendix a list of the resulting equations is given with frequency-independent parameters when the number of adsorbed intermediates is less than four.

Experimental

Instrumentation, cells and electrodes. The instrumentation setup has been described elsewhere.[9] The cell was a Metrohm titration vessel with a specially designed lid. A calomel reference electrode with saturated NaCl solution, SSCE ($E = 0.236$ V vs. NHE), and a platinum counter-electrode were used throughout the work. The counter-electrode was separated from the eletrolyte by a glass frit to avoid contamination. The electrolyte solution was bubbled with purified nitrogen for at least 40 min before the experiment was started, and a nitrogen atmosphere was maintained in the cell during the experiments.

Rotating disc eletrodes with a surface of 0.2 cm^2 were prepared from 99.99 % pure zinc rods (Johnson Matthey Chemical Ltd.). The electrodes were moulded in epoxy, exposing only the circular disc surface. Before measurement, the electrode was wet-ground on silicon carbide paper (1000 and 4000 mesh), rinsed with doubly distilled water and immediately placed in the cell. The rotation speed of the electrode was 0 or 50 rps.

Chemicals. 2 M perchlorate solution was prepared from p.a. $NaClO_4$ (Merck) and doubly distilled water. 0.67 M sulfate solution was prepared in the same way from p.a. grade chemicals (Merck) of Na_2SO_4. The sulfate solution was diluted to 0.2 M with the perchlorate solution. The pH of the solution was adjusted to pH 3.0 by addition of perchloric acid or sodium hydroxide of the same ion strength as the electrolyte. The pH was controlled by a pH-stat system from Radiometer (pH-meter 84, titrator TTT 80 and autoburette ABU 80) together with a combined glass electrode GK 2401c. No zinc salt was added to the solution, but approximately 1 mM zinc ions were generated at high anodic potentials during the pretreatment of the electrode.

Impedance measurements. The impedance was recorded after 5 min of pre-polarisation at the same potential as the impedance measurement was conducted. Data were collected from 100 kHz to 10 mHz with 10 points per decade of frequency. The amplitude of the input signal was 5 mV.

Results and discussion

The impedance behaviour of three mechanisms M1, M2 and M3 with no, one and two adsorbed intermediates, respectively, was studied by simulation. These mechanism are dissolution/deposition reactions in which a solid metal is oxidised electrochemically to a soluble divalent cation or *vice versa.* The M1 mechanism is the simple two-electron transfer reaction and the M2 mechanisms is the two-step consecutive electron transfer reaction where the intermediate is assumed to be adsorbed on the surface only. In the M3 mechanism the Volmer–Heyrovsky mechanism is assumed to occur in parallel to the M2 mechanism. The metal ions are supposed to react on the free metal surface only, whereas the hydrogen ions can be reduced at the free surface or at sites occupied by adsorbed hydrogen. Diffusion-limited reaction rates occur only for cathodic reaction steps in which soluble species are reactants. Surface diffusion of adsorbed intermediates is assumed to be fast enough to reveal their kinetics. Thus, the rates of anodic reaction steps are not

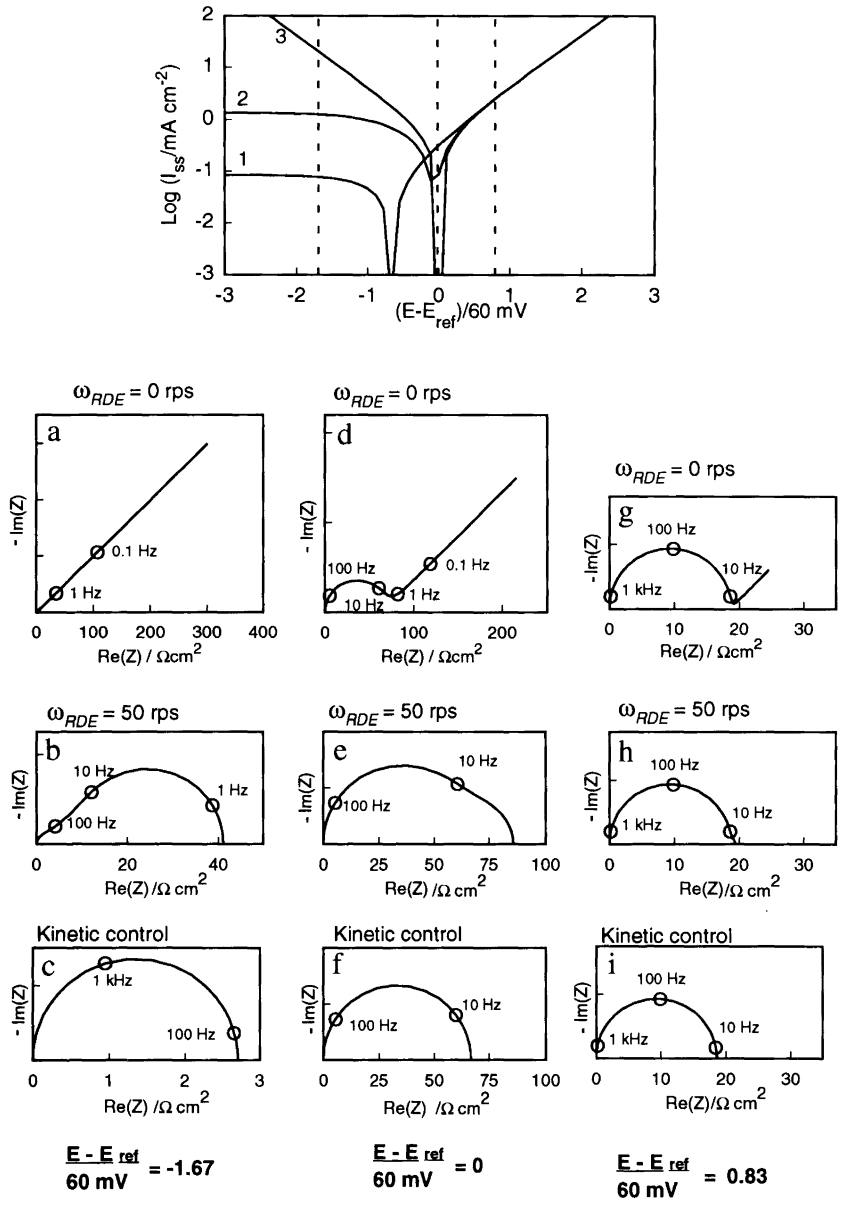

Fig. 1. Top: Simulated steady-state polarisation curves of the M1 mechanism at different hydrodynamic conditions. (1) $\omega_{RDE} = 0.2$ rps; (2) $\omega_{RDE} = 50$ rps; (3) kinetic control. (a)–(i) Simulated impedance spectra of the M1 mechanism at potentials and hydrodynamic conditions given in the figure. (The scale and units of the *y*-axis of the impedance diagrams are the same as for the *x*-axis.)

hindered by diffusion, since the reactants of the anodic reaction will not be depleted. In the simulations presented below the concentration of soluble species was set to 1 mM. The rate constants and other parameters used are listed in Table 1. In order to compare the results for the different mechanisms, the potential scale in the polarisation diagrams has been normalised to the anodic Tafel slope at high overpotentials for each mechanism. Thus the potential scale of the M1 mechanism is given in units of ln 10 RT/F and for the other mechanisms the unit is 2ln 10 RT/F.

M1

$$Me_s \underset{k_{-1}}{\overset{k_1}{\rightleftharpoons}} Me^{2+}_{aq} + 2e^-$$

M2

$$Me_s \underset{k_{-1}}{\overset{k_1}{\rightleftharpoons}} Me^{+}_{ad} + e^-$$

$$Me^{+}_{ad} \underset{k_{2}}{\overset{k_2}{\rightleftharpoons}} Me^{2+}_{aq} + e^-$$

M3

$$Me_s \underset{k_{-1}}{\overset{k_1}{\rightleftharpoons}} Me^{+}_{ad} + e^-$$

$$Me^{+}_{ad} \underset{k_{-2}}{\overset{k_2}{\rightleftharpoons}} Me^{2+}_{aq} + e^-$$

$$H^{+}_{aq} + e^- \underset{k_{-3}}{\overset{k_3}{\rightleftharpoons}} H_{ad}$$

$$H^{+}_{aq} + H_{ad} + e^- \xrightarrow{k_4} H_2$$

In Fig. 1 the logarithm of the steady-state current density, I_{ss}, as a function of the potential for the M1 mechanism is shown at different diffusion layer thicknesses corresponding to 0.2 and 50 rps in the Levich equation. For comparison the kinetically derived current is also plotted. Cole–Cole plots of the impedance simulated at three different potentials are also shown, Fig. 1(1a–1i). At cathodic potentials the charge-transfer loop is masked by the Warburg impedance (a), which becomes depressed as the diffusion layer is reduced (b). As the potential is increased in the anodic direction the Warburg impedance becomes less important and the charge-transfer loop is clearly visible (d). Simulating the impedance at a higher rotation speed of the electrode ($\omega_{RDE} = 50$ rps) eliminates the Warburg tail (e). However, pure charge-transfer kinetics is still not obtained (f). At anodic potentials, 50 mV, the effect of diffusion is only observed at stationary conditions (g)–(i).

The M2 mechanism was simulated by using the same values of the rate constants for the slow step at $E - E_{ref} = 0$ as for the M1 mechanism. In Figs. 2 and 3 the potential dependence of the steady-state currents is shown as in Fig. 1, together with the potential dependence of the charge-transfer resistance, R_{ct}, and the polarisation resistance, R_p, when diffusion is unimportant. Fig. 2 refers to the case when the first step (K_1/K_{-1}) is in pseudo-equilibrium at $E - E_{ref} = 0$, and Fig. 3 to the case when the second step (K_2/K_{-2}) is in pseudoequilibrium at $E - E^\circ = 0$. The difference between R_{ct} and R_p close to E_{ref} reflects the large contribution of the adsorption kinetics. Note that under kinetic control the potential dependence of log I_{ss}, R_{ct} and R_p of this mechanism is symmetric around E_{ref}, when E_{ref} is the same for the two steps. This makes it impossible, from the impedance data as well as from the steady-state data, to tell whether the first or second step is rate-determining. The symmetry is broken when diffusion of Me^{2+} becomes important, and it is therefore interesting to study the impedance taking the diffusion into account. The impedance of the M2 mechanism, when $K_{-1} \gg K_{-2}$ and when the diffusion of Me^{2+} is important, is similar to the impedance of the M1 mechanism, but one difference should be noted. In the M2 mechanism a coupling between the adsorption and diffusion processes occurs.

At cathodic potentials, Figs. 2a–2c, both the charge-transfer and the adsorption kinetics are masked by the Warburg impedance as for the M1 mechanism. When the overpotential is zero the coupling effect is seen as an

Table 1. The rate constants and other parameters used in the simulations.

	Mechanism				
	M1	M2		M3	
Parameter		First step rds	Second step rds		Zinc dissolution
$c_{Me^{2+}}$/mol cm^{-3}	10^{-6}	10^{-6}	10^{-6}	10^{-6}	10^{-5}
c_{H^+}/mol cm^{-3}				10^{-6}	10^{-6}
k_1^*/k^*_{-1}/cm s^{-1}	$10^{-9}/10^{-3}$	$10^{-9}/10^{-9}$	$10^{-7}/10^{-7}$	$2\times10^{-9}/10^{-9}$	$6.91\times10^{-8}/1.54\times10^{-8}$
k_2^*/k^*_{-2}/cm s^{-1}		$10^{-7}/10^{-1}$	$10^{-9}/10^{-3}$	$2.5\times10^{-8}/2\times10^{-9}$	$1.07\times10^{-9}/7.33\times10^{-6}$
k_3^*/k^*_{-3}/cm s^{-1}				$5\times10^{-3}/10^{-9}$	1.18×10^{-7}/—
k_4^*/k^*_{-4}/cm s^{-1}				2×10^{-3}/—	$1.71\times10^{-3}/5.33\times10^{-9}$
k_5^*/k^*_{-5}/cm s^{-1}					1.71×10^{-4}/—
$\alpha_1, \alpha_2, \ldots$	0.5	0.5, 0.5	0.5, 0.5	0.5, 0.5, 0.5, 0.5	0.5, 0.5, 0.5, 0.5, 0.5
β_1, β_2/mol cm^{-2}	6×10^{-9}	$6\times10^{-9}, 6\times10^{-9}$	$6\times10^{-9}, 6\times10^{-9}$	$6\times10^{-9}, 6\times10^{-9}$	$6\times10^{-9}, 6/10^{-9}$
C_{dl}/μF cm^{-2}	80	80	80	80	160

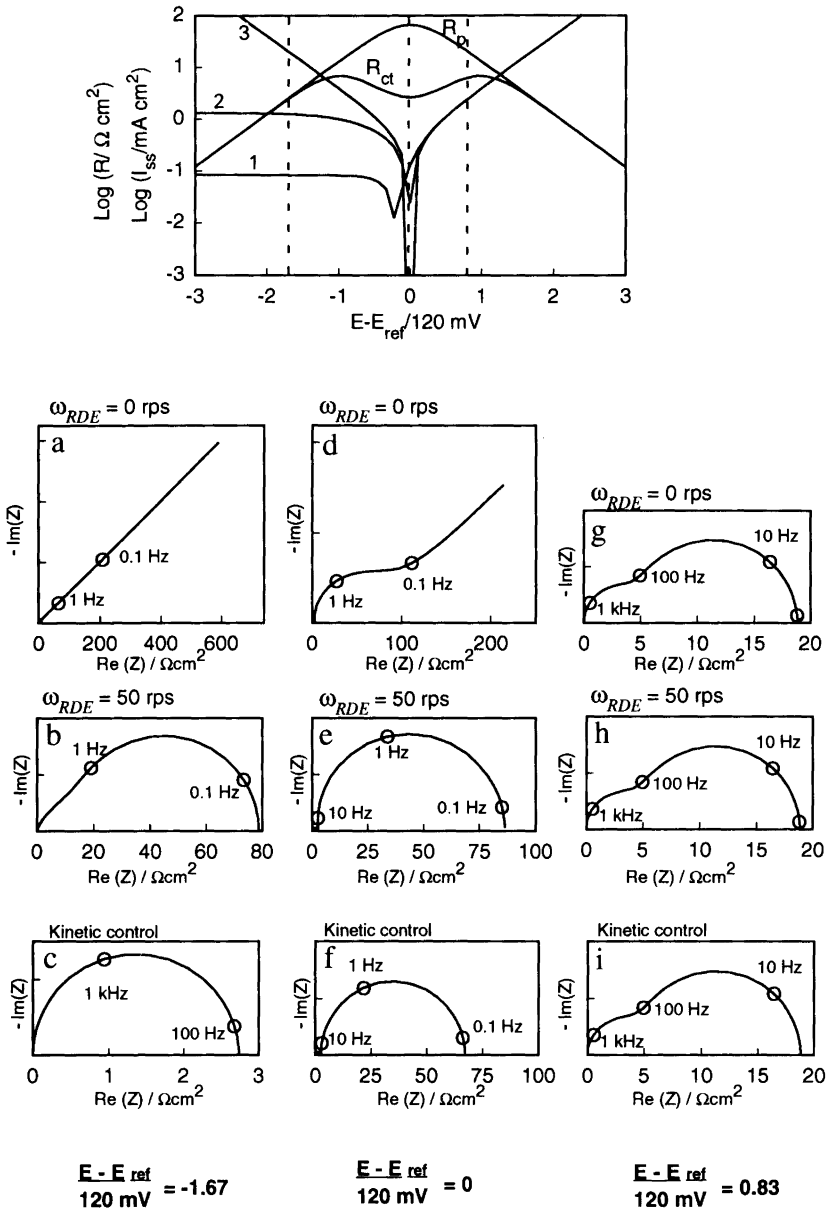

Fig. 2. Top: Simulated steady-state polarisation curves of the M2 mechanism with the first step (K_1/K_{-1}) in pseudo-equilibrium at different hydrodynamic conditions. (1) $\omega_{RDE} = 0.2$ rps; (2) $\omega_{RDE} = 50$ rps; (3) kinetic control. (a)–(i) Simulated impedance spectra of the M2 mechanism with the first step (K_1/K_{-1}) in pseudo-equilibrium at potentials and hydrodynamic conditions given in the figure. (The scale and units of the *y*-axis of the impedance diagrams are the same as for the *x*-axis.)

enlargement of the semicircle, Figs. 2d and 2e, compared to the semicircle obtained under kinetic control, Fig. 2f. The large semi-circle in Fig. 2f is associated with the adsorption kinetics, and the charge-transfer loop is hardly seen in the high-frequency part of this spectra. At anodic potentials the impedance spectrum are not influenced by the diffusion, Figs. 2g–2i.

The impedance behaviour of the M2 mechanism when the first step is rate-determining ($K_{-2} \gg K_{-1}$) differs considerably from the previous case. The impedance at cathodic potentials, Figs. 3a and 3b, is now to a much larger extent determined by the charge-transfer kinetics, although the true charge-transfer resistance will be overestimated if the usual extrapolation is carried out. Under these conditions the coupling between the adsorption and diffusion processes gives rise to a double point in the spectra. This behaviour has not been reported earlier. In order to elucidate this adsorption/diffusion coupling further the faradaic impedance was also simulated, which eliminates interference with the charge-transfer loop (Fig. 4). The impedance shows a full 360° loop in the frequency range where the coupling effect is pronounced. This can be understood from a theoretical point of view by a sign analysis of the parameters in eqn. (13). It can be

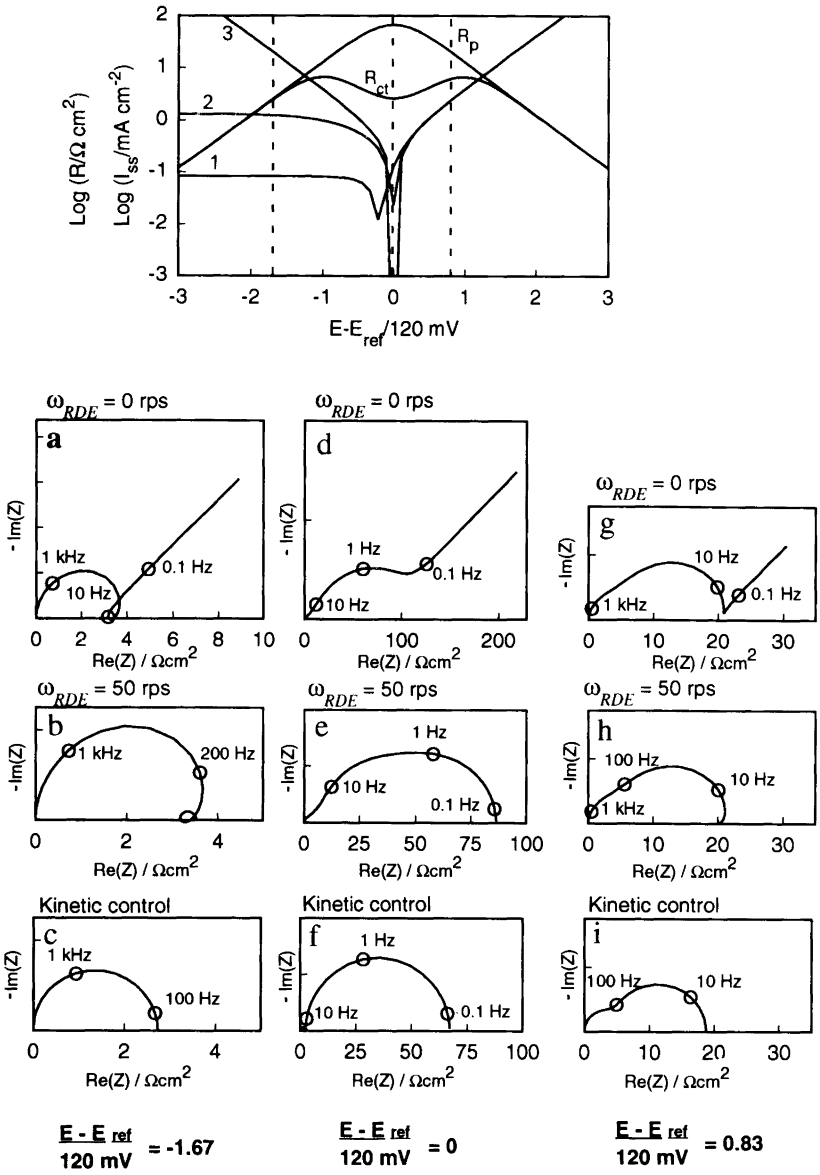

Fig. 3. Top: Simulated steady-state polarisation curves of the M2 mechanism with the second step (K_2/K_{-2}) in pseudo-equilibrium at different hydrodynamic conditions. (1) $\omega_{RDE} = 0.2$ rps; (2) $\omega_{RDE} = 50$ rps; (3) kinetic control. (a)–(i) Simulated impedance spectra of the M2 mechanism with the second step (K_2/K_{-2}) in pseudo-equilibrium at potentials and hydrodynamic conditions given in the figure. (The scale and units of the *y*-axis of the impedance diagrams are the same as for the *x*-axis.)

shown that for this particular case, where there is a well defined rate-determining step in the M2 mechanism, the coupling term, C_1, is the only parameter that changes sign as the rate-determining step is changed.

Figs. 3d and 3e show the impedance simulated at E°. The spectra are hard to distinguish from the corresponding spectra in Fig. 2. However, a closer look reveals that the coupling effect now acts in the opposite direction, i.e., the semicircle is slightly depressed. At anodic potentials the diffusion is more pronounced, Fig. 3(g), compared to the case in Fig. 2. In the presence of convection the Warburg tail disappears, but pure kinetic behaviour is not obtained, Figs. 3h and 3i. Even if the spectra in Figs. 3h and 3i are fairly similar it should be pointed out that the impedance is independent of the diffusion layer thickness. This is quite remarkable, since the only diffusion process considered was in the cathodic reaction step of Me^{2+} ions to Me^{+}_{ad}, which have negligible influence on the steady-state current at this potential (100 mV from E_{ref}). The spectra simulated under kinetic control, Figs. 3c, 3f and 3i, are the same as before, Figs. 2c, 2f and 2i.

The next case of interest was the impedance of a reaction where an inductive relaxation of an adsorbed intermediate was coupled to the diffusion process. Although the M2 mechanism may exhibit inductive properties, it was not chosen because of (1) the small potential region

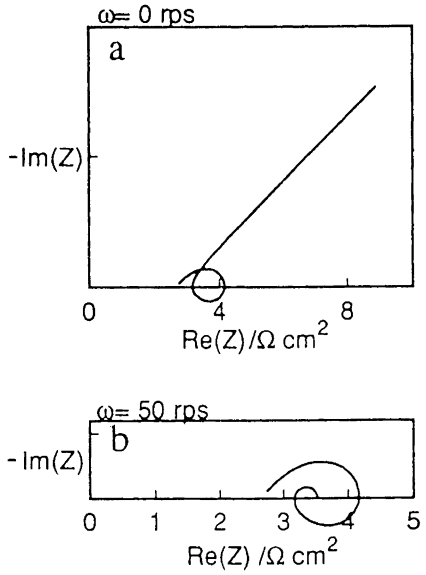

Fig. 4. The faradaic impedance ($C_{dl}=0$) of the M2 mechanism with the second step (K_2/K_{-2}) in pseudo-equilibrium at $E-E^\circ=-200$ mV; (a) $\omega_{RDE}=0$ rps; (b) $\omega_{RDE}=50$ rps. (The scale and units of the *y*-axis of the impedance diagrams are the same as for the *x*-axis.)

where the relaxation of the intermediate is inductive and (2) the small diameter of the loop obtained when simulating the process with $\alpha_c=1/2$. Instead a parallel two-step process with an additional adsorbed intermediate was added to the M2 mechanism, for example the hydrogen evolution reaction, the M3 mechanism. It was found that this mechanism exhibited inductive behaviour for various sets of rate constants. This is seen in the upper diagram in Fig. 5, where $R_p < R_{ct}$ at anodic potentials. Simulating the M3 mechanism at cathodic potentials and taking the diffusion of the two species into account the impedance spectra show the usual characteristics for diffusion controlled reactions, a Warburg tail, Fig. 5a, which becomes depressed when the diffusion layer is decreased by convention, Fig. 5b. At anodic potentials the relaxations from the adsorbed intermediates become visible (inductive). As in the case for the M2 mechanism with the first step rate-determining, the Warburg impedance can be observed at very high anodic potentials, where the major part of the current is determined by the anodic reactions, Fig. 5g. When the diffusion layer is reduced by convection, Fig. 5h, the Warburg tail becomes depressed into a semicircle. This semicircle becomes more and more insensitive to the convection as the thickness of the diffusion layer diminishes. This is shown in Fig. 5h where the impedance is plotted as a function of the rotation speed. The spectra in Fig. 5h resembles to a great extent experimental spectra, obtained with a rotating disc electrode, of the zinc dissolution reaction in slightly acidic solutions.[4,8,9]

The reason for introducing the hydrogen evolution in parallel to the dissolution reaction descends from the fact that adsorption of hydrogen plays an important role in the electrocrystallisation of zinc in an acidic medium.[4,5,11]

It was in fact shown that the coverage of H_{ad} at the equilibrium potential of the Zn/Zn^{2+} electrode was close to 1.[5] At cathodic potentials the hydrogen evolution takes place and at anodic potentials the rate of hydrogen reduction is lowered. The desorption of H_{ad} as the potential is made anodic can explain the low Tafel slopes obtained experimentally (<30 mV). Neither the impedance spectra nor the steady-state current showed any rotation speed dependence above 30 rps. Since it is well established that the anodic dissolution of zinc contains adsorbed intermediates, we investigated the possibility of a coupling between adsorption of intermediates and diffusion of soluble species towards the electrode. Several mechanisms were evaluated and compared to experimental data. The mechanism that showed the best correspondance with experimental data was M4, where Zn_k is a kink site or a

Zinc dissolution

$$Zn_s \underset{k_{-1}}{\overset{k_1}{\rightleftharpoons}} Zn_{ad}^{+} + e^-$$

$$Zn_{ad}^{+} \underset{k_{-2}}{\overset{k_2}{\rightleftharpoons}} Zn_{aq}^{2+} + e^-$$

$$Zn_k Zn_{ad}^{+} \xrightarrow{k_3,\ \text{autocatalytic}} Zn_{aq}^{2+} + Zn_{ad}^{+} + 2e^-$$

$$H_{aq}^{+} + e^- \underset{k_{-4}}{\overset{k_4}{\rightleftharpoons}} H_{ad}$$

$$H_{aq}^{+} + H_{ad} + e^- \xrightarrow{k_5} H_2$$

defect on the surface. Besides the consecutive mechanism (M2) it contains an autocatalytic step through which most of the dissolution takes place. The presence of an autocatalytic step has been proposed for both the dissolution and deposition of zinc.[5,8,9,11]

In Fig. 6 the experimental spectra are shown along with theoretical simulations. In the upper part of the figure the theoretical polarisation curve is shown together with experimental steady-state currents, obtained with a RDE, $\omega_{RDE}=50$ rps. At the stationary electrode the current density was somewhat higher at potentials close to the corrosion potential, as indicated in the figure. The simulations of the impedance spectra were made so that an agreement with experimental R_{ct}-values was established. All simulations were make with the same set of rate constants (Table 1).

The experimental impedance spectra are characterised by the charge-transfer loop in the kHz region, the inductive loop in the 10 Hz region (not fully resolved at low overpotentials) and a capacitive loop or a distorted Warburg tail in the low-frequency region depending on the hydrodynamic conditions, Figs. 6a–6c. The simulated spectra show a good agreement with experimental spectra, although some deviation is observed at low frequencies for the stationary electrode. In Fig. 6e spectra at four different rotation speeds are shown, simulated at 50, 60,

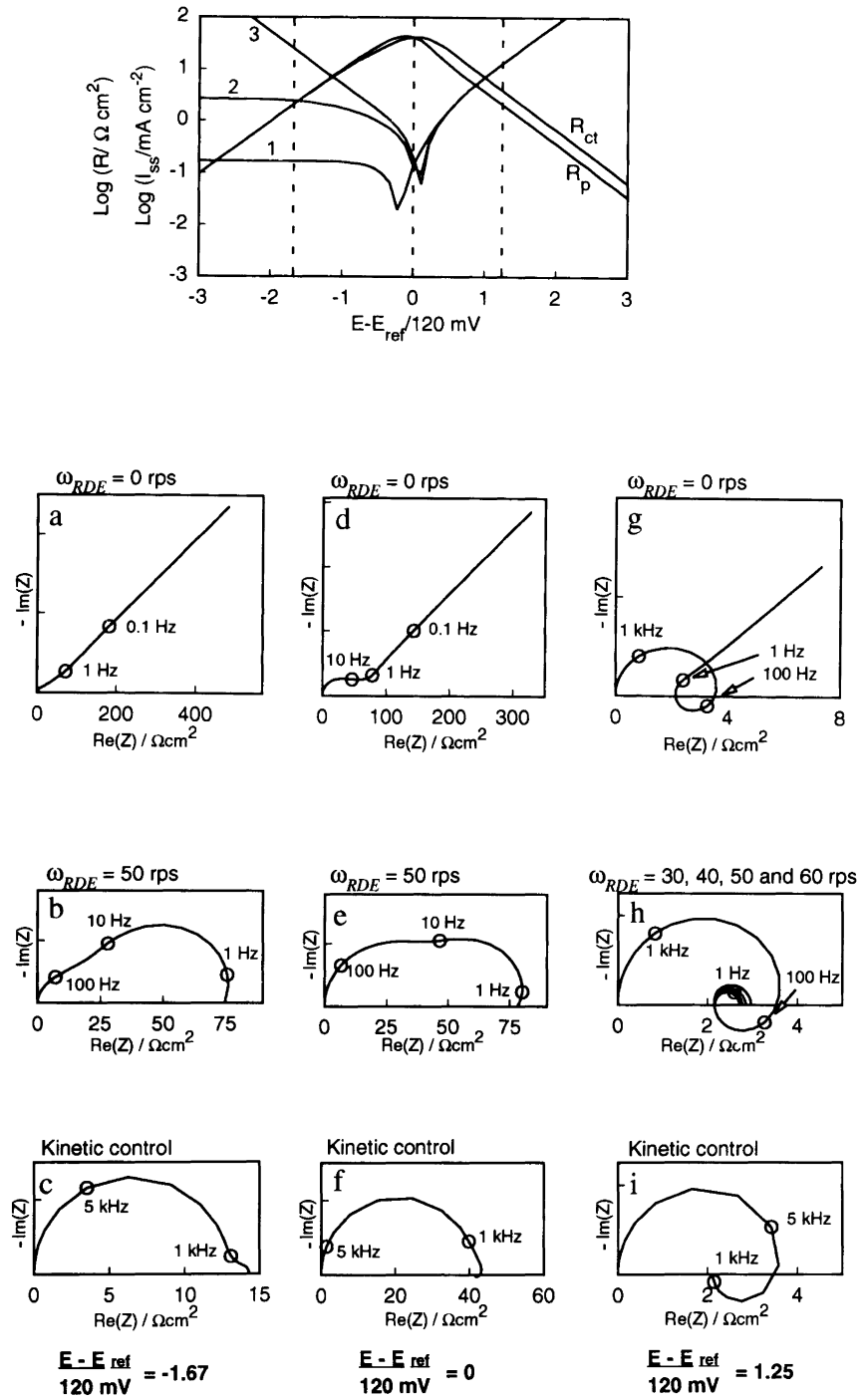

Fig. 5. Top: Simulated steady-state polarisation curves of the M3 mechanism at different hydrodynamic conditions. (1) $\omega_{RDE} = 0.2$ rps; (2) $\omega_{RDE} = 50$ rps; (3) kinetic control. (a)–(i) Simulated impedance spectra of the M3 mechanism at potentials and hydrodynamic conditions given in the figure. (The scale and units of the *y*-axis of the impedance diagrams are the same as for the *x*-axis.)

70 and 80 rps, to indicate the relatively small dependence on the rotation speed of the electrode.

The results show that it is possible to interpret the experimental impedance at low frequencies as an effect of diffusion of soluble species towards the electrode.

Conclusions

Although experimental data are not influenced by changes in the hydrodynamic conditions, it has been shown in the present paper that diffusion effects can remain even at

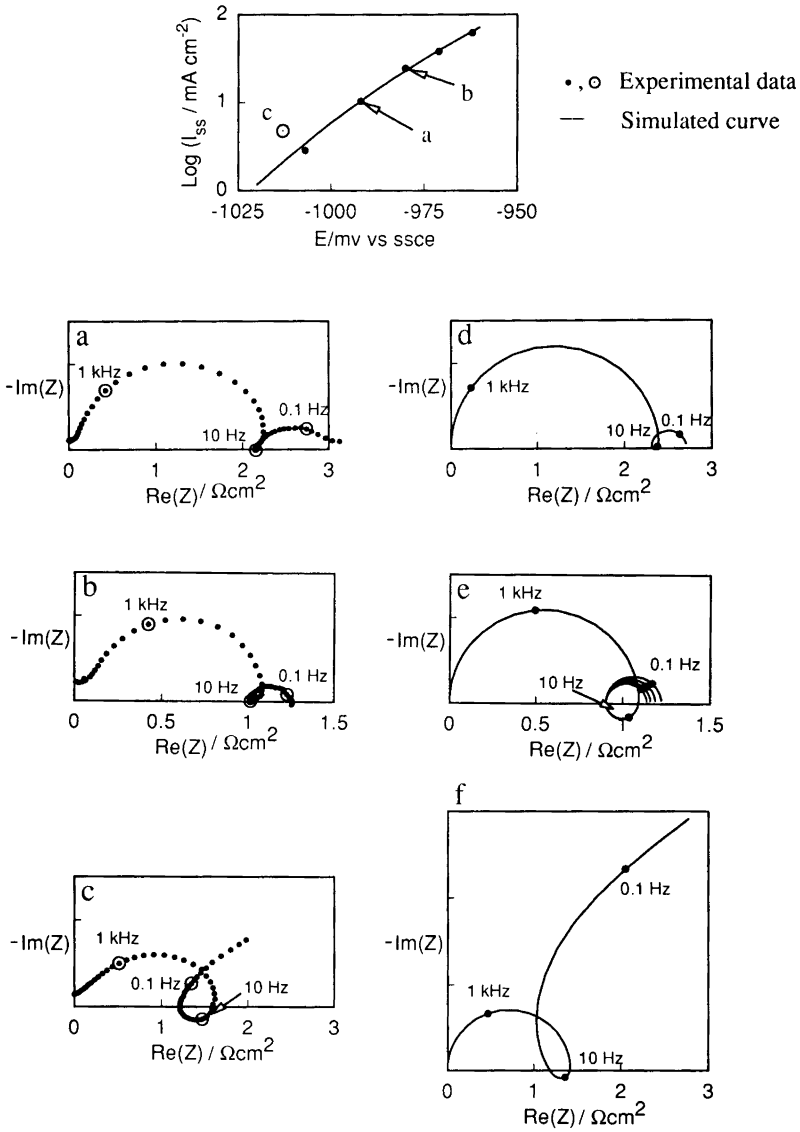

Fig. 6. Top: Experimental steady-state current at different potentials obtained in 0.2 M sulfate solution. ● $\omega_{RDE} = 50$ rps; ⊙ $\omega_{RDE} = 0$ rps. Simulated steady-state polarisation curve (—). Below to the left: Experimental impedance spectra obtained in 0.2 M sulfate solution. (a,b) $\omega_{RDE} = 50$ rps; (c) $\omega_{RDE} = 0$ rps. Below to the right: Simulated impedance spectra. (d,e) $\omega_{RDE} = 50$ rps; (f) $\omega_{RDE} = 0$ rps. (The scale and units of the *y*-axis of the impedance diagrams are the same as for the *x*-axis.)

anodic potentials owing to the specific coupling between the adsorption and diffusion processes. For the anodic dissolution of zinc in slightly acidic solutions it was shown that the impedance at low frequencies could be interpreted as the coupling between the adsorption and diffusion even under hydrodynamic conditions.

Appendix

The faradaic impedance can be written as eqn. (A1). Let m represent the number of adsorbed intermediates, $n - m$ the number of diffusing species and $i = 1, ..., m; j = 1, ..., m; k = m + 1, ..., n$. Then for $m = 1 - 3$ we have the following sets of equations.

$$Y_f = \frac{\dfrac{1}{R_{ct}} + Y_{ads}}{1 - \sigma'/\sqrt{\omega} - \sigma/\sqrt{\omega}} \qquad \text{(A1)}$$

$m = 1$:

$$Y_{ads} = -\frac{\partial I_f}{\partial \theta_1} \frac{a_1}{J_{1,1} - j\omega}$$

$$\sigma' = -\frac{1}{F} \frac{\partial I_f}{\partial \theta_1} \frac{\sum_k R_{1,k} \dfrac{Y_k(\omega)}{(jD_k)^{1/2}}}{J_{1,1} - j\omega}$$

$$\sigma = \frac{1}{F} \sum_k \left(\frac{\partial I_f}{\partial c_k} \frac{Y_k(\omega)}{(jD_k)^{1/2}} \right)$$

$m = 2$:

$$Y_{ads} = \frac{\sum_i \left[\frac{\partial I_f}{\partial \theta_i} \sum_j (-1^{(i+j-1)} S_{j,i} a_j) + j\omega a_i \right]}{|J| - j\omega V - \omega^2}$$

$$\sigma' = \frac{1}{F} \frac{\left[\sum_i \left[\frac{\partial I_f}{\partial \theta_i} \sum_j \left(-1^{(i+j-1)} S_{j,i} \sum_k \left(R_{j,k} \frac{Y_k(\omega)}{(jD_k)^{1/2}} \right) \right) \right] + j\omega \sum_k \left(R_{i,k} \frac{Y_k(\omega)}{(jD_k)^{1/2}} \right) \right]}{|J| - j\omega V - \omega^2}$$

$$\sigma = \frac{1}{F} \sum_m \left(\frac{\partial I_f}{\partial c_m} \frac{Y_m(\omega)}{(jD_m)^{1/2}} \right)$$

$m = 3$

$$Y_{ads} = \frac{\sum_i \left[\frac{\partial I_f}{\partial \theta_i} \left(\sum_j \{ -1^{(i+j)} a_j (j\omega S_{j,i} - |J|_{j,i}) \} + \omega^2 a_i \right) \right]}{|J| - j\omega U - \omega^2 V + j\omega^3}$$

$$\sigma' = \frac{1}{F} \frac{\left[\sum_i \left[\frac{\partial I_f}{\partial \theta_i} \left(\sum_j \left\{ -1^{(i+j)} (j\omega S_{j,i} - |J|_{j,i}) \sum_k R_{j,k} \frac{Y_k(\omega)}{(jD_k)^{1/2}} \right\} + \omega^2 \sum_k R_{i,k} \frac{Y_k(\omega)}{(jD_k)^{1/2}} \right) \right] \right]}{|J| - j\omega U - \omega^2 V + j\omega^3}$$

$$\sigma = \frac{1}{F} \sum_k \left(\frac{\partial I_f}{\partial c_k} \frac{Y_k(\omega)}{(jD_k)^{1/2}} \right)$$

The coefficients are defined as follows:

$S_{i,j} = J_{i,j}$; $i \neq j$, not$(i = 1 \wedge j = 3)$, not$(i = 3 \wedge j = 1)$

$S_{i,i} = \sum_{i \neq j} J_{j,j}$

$S_{1,3} = -J_{1,3}$

$S_{3,1} = -J_{3,1}$

$|J|$ = The determinant of the J-matrix without the jω-terms

$|J|_{i,j}$ = The subdeterminant of the J-matrix without the jω-terms when the ith row and jth column are excluded

$U = \sum_i |J|_{i,i}$

$V = \sum_i J_{i,i}$

$(j\omega D)^{1/2} = \left(\frac{\omega D}{2} \right)^{1/2} (1 + j)$

$Y_k(\omega) = 1$; for infinite diffusion layer

$Y_k(\omega) = \tanh \left[\delta_k \left(\frac{j\omega}{D_k} \right)^{1/2} \right]$; for finite diffusion layer

The following relation is useful for calculation of $Y(\omega)$:

$$\tanh(a + jb) = \frac{\sinh(2a)}{\cosh(2a) + \cos(2b)} + j \frac{\sin(2b)}{\cosh(2a) + \cos(2b)}$$

References

1. Macdonald, D. D. *Electrochim. Acta 35* (1990) 1509.
2. Wiart, R. *Electrochim. Acta 35* (1990) 1587.
3. Keddam, M., Mattos, O. R. and Takenouti, H. J. *J. Electrochem. Soc. 128* (1981) 257, 266.
4. Cachet, C. and Wiart, R. *J. Electroanal. Chem. 111* (1980) 235.
5. Cachet, C. and Wiart, R. *J. Electroanal. Chem. 129* (1981) 103.
6. Armstrong, R. D., Firman, R. E. and Thirsk, H. R. *Faraday Discuss. Chem. Soc. 56* (1973) 244.
7. Epelboin, I. and Keddam, M. *J. Electrochem. Soc. 117* (1970) 1052.
8. Deslouis, C., Deprat, M. and Tournillon, C. *Corrosion Sci. 29* (1989) 13.
9. Ahlberg, E. and Anderson, H. *Acta Chem. Scand. 46* (1992) 15.
10. Ahlberg, E. and Anderson, H. *Acta Chem. Scand. 46* (1992) 1.
11. Epelboin, I., Ksouri, M. and Wiart, R. *J. Electrochem. Soc. 122* (1975) 1206.

Received February 4, 1993.